MODELLING SIEVE TRAY HYDRAULICS USING COMPUTATIONAL FLUID DYNAMICS

R. Krishna and J.M. van Baten

Department of Chemical Engineering, University of Amsterdam,
Nieuwe Achtergracht 166, 1018 WV Amsterdam, The Netherlands

ABSTRACT

The ability of Computational Fluid Dynamics (CFD) to model the complex two-phase hydrodynamics of sieve trays is examined. The key to a proper description of the flow is the estimation of the momentum exchange, or drag, coefficient between the gas and liquid phases. In the absence of sound theoretical models, empirical correlations for the average gas fraction on the tray, such as those of Bennet, Agrawal and Cook (*A.I.Ch.E.J.*, **29** (1983) 434), can be used to estimate the drag coefficient. Transient simulations of sieve trays of 0.3 m and 0.9 m in diameter reveal the chaotic, three-dimensional character of the flow and the existence of circulation patterns in all three dimensions. The CFD simulations underline the limitations of simpler approaches wherein the flow is assumed to be two-dimensional or where the interaction of the liquid phase with the gas phase is either ignored completely or simplified greatly. The major advantage of the CFD approach is that geometry and scale effects are properly encapsulated and do not require further inputs. It is concluded that CFD can be a powerful investigative and design tool for sieve tray columns.

Keywords: Computational fluid dynamics, sieve trays, clear liquid height, froth height, froth density, scale effects, liquid circulations

INTRODUCTION

Distillation is the most widely used separation technique and is usually the first choice for separating mixtures. Only when distillation fails does one look for other separation alternatives. One of the major factors that favour distillation is the fact that large diameter columns can be designed and built with confidence. Sieve tray distillation columns are widely used in industrial practice and the description of the hydrodynamics of sieve trays is of great importance. A proper prediction of the sieve tray hydraulics is necessary for the prediction of separation efficiency and overall tray performance. For a given set of operating conditions (gas and liquid loads), tray geometry (column diameter, weir height, weir length, diameter of holes, fractional hole area, active bubbling area, downcomer area) and system properties, it is required to predict the flow regime prevailing on the tray, liquid hold-up, clear liquid height, froth density, interfacial area, pressure drop, liquid entrainment, gas and liquid

phase residence time distributions and the mass transfer coefficients in either fluid phase. According to many industrial experts, a lack of in-depth understanding of the processes occurring within a distillation column is a significant barrier to the further improvement of equipment performance [1]. In 1986, in the preface to his influential book, M.J. Lockett [2] wrote “Sieve tray decks are, after all, hardly more than sheets of metal with a few holes punched in them. This of course is part of the fascination – that the behaviour of something so simple can be so difficult to predict with regards to its hydrodynamic and mass transfer performance.” Design of sieve tray distillation columns is essentially empirical in nature [2-7].

In recent years, there has been considerable academic and industrial interest in the use of Computational Fluid Dynamics (CFD) to model two-phase flows in process equipment [8-21]. CFD techniques have been used to model bubble formation and rise in liquids and powders [8,9] and to describe the hydrodynamics of bubble columns [10-14] and fluidised beds [15,16]. An important advantage of CFD techniques is that geometry and scale effects are “automatically” accounted for [14,16].

There have been some recent attempts to model sieve tray hydrodynamics using CFD [17-21]. Mehta et al. [17] have analysed the liquid phase flow patterns on a sieve tray by solving the time-averaged equations of continuity of mass and momentum only for the liquid phase. Interactions with the vapour phase are taken account of by use of interphase momentum transfer coefficients determined from empirical correlations. Liu et al. [18] attempt to model the two-phase flow behaviour using a two-dimensional model, focussing on the description of the hydrodynamics along the liquid flow path, ignoring the variations in the direction of gas flow along the height of the dispersion. Van Baten et al. [19-21] use fully three-dimensional transient simulations to describe the hydrodynamics of sieve trays.

The objective of the present communication is to examine the power, and limitations of CFD techniques in describing sieve tray hydraulics. We review and extend our previous CFD approach [19-21] to the description of liquid phase residence time distribution (RTD) and to the influence of scale effects. We begin with a 2D analysis of liquid phase channelling and bypassing on a tray.

TWO-DIMENSIONAL CFD ANALYSIS OF LIQUID PHASE CHANNELLING

Before attempting to model the complex gas-liquid tray hydrodynamics, let us consider CFD simulation of a simple case of flow of liquid across a round tray with the dimensions specified in Fig. 1 (a). A total of $48\times60 = 1680$ grid cells of warped configuration are used to cover the tray geometry. The liquid load per unit weir length is taken to be 8.25×10^{-4} m^3/s/m, corresponding to an inlet liquid velocity of 0.055 m/s. The mass and momentum conservation equations are:

$$\frac{\partial \rho_{\mathrm{L}}}{\partial t} + \nabla \bullet \left(\rho_{\mathrm{L}} \mathbf{u}_{\mathrm{L}}\right) = 0 \qquad (1)$$

$$\frac{\partial \rho_{\mathrm{L}} \mathbf{u}_{\mathrm{L}}}{\partial t} + \nabla \bullet \left(\rho_{\mathrm{L}} \mathbf{u}_{\mathrm{L}} \mathbf{u}_{\mathrm{L}} - \mu_{\mathrm{L}} \left(\nabla \mathbf{u}_{\mathrm{L}} + \left(\nabla \mathbf{u}_{\mathrm{L}} \right)^{\mathrm{T}} \right) \right) = -\nabla p + \rho_L \mathbf{g} \qquad (2)$$

where ρ_{L}, $\mathbf{u}_{\mathrm{L}}$, and μ_{L} represent, respectively, the macroscopic density, velocity, and viscosity of the liquid phase, p is the pressure, and $\mathbf{g}$ is the gravitational acceleration. The turbulent contribution to the stress tensor is evaluated by means of low Reynolds number variant of the k-ε model [22], using standard single-phase parameters C_{μ}=0.09, $C_{1\varepsilon}$=1.44, $C_{2\varepsilon}$=1.92, σ_{k} = 1 and σ_{ε} = 1.3.

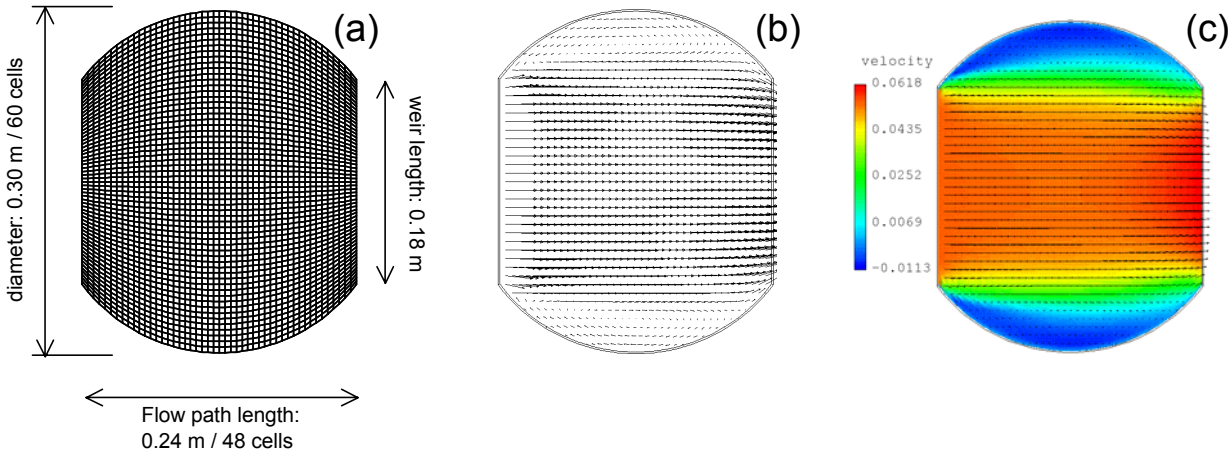

Figure 1. 2D Simulation of liquid flow across a tray of 0.3 m diameter. (a) computational grid. (b) Steady-state velocity vectors shown as arrows. (c) Representation of velocities in colour scheme; colour scale shown on the left.

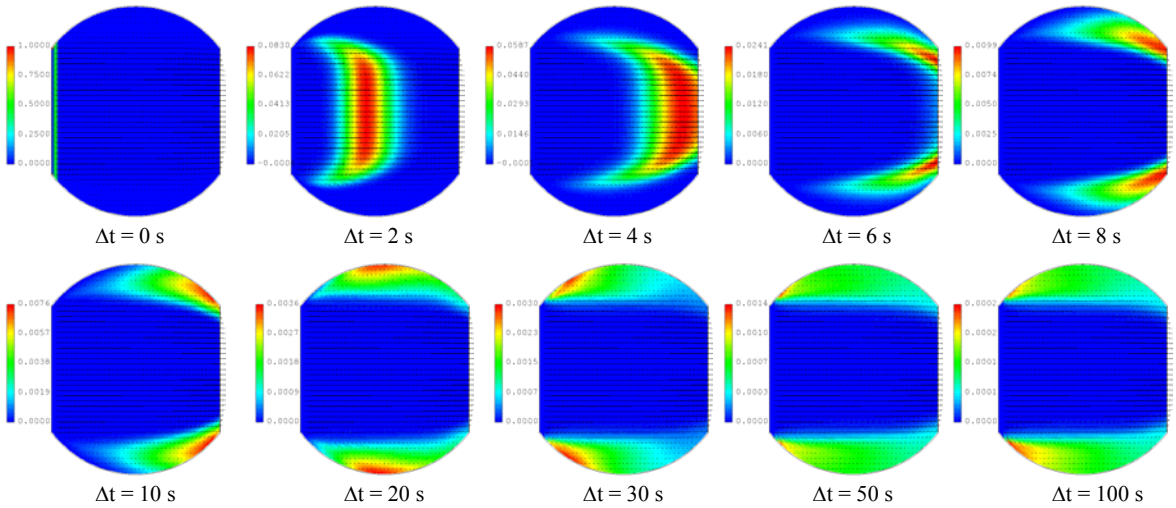

Figure 2. Snapshots showing the movement of colour tracer across the tray. Highest tracer concentration is denoted by red. Blue areas do not encounter tracer. The shades of colours in between blue and red denote the tracer concentrations. The colour scales are indicated at the left of each snapshot.

A commercial CFD package CFX 4.2 of AEA Technology, Harwell, UK, was used to solve Eqs (1) and (2) of continuity and momentum. This package is a finite volume solver, using body-fitted grids. Discretisation of the equations at the grid is performed using a finite differencing (finite volume) method. Physical space is mapped to a rectangular computational space. Velocity vector equations are treated as scalar

equations, one scalar equation for each velocity component. All scalar variables are discretised and evaluated at the cell centres. Velocities required at the cell faces are evaluated by applying an improved Rhie-Chow interpolation algorithm [23]. Transport variables such as diffusion coefficients and effective viscosities are evaluated and stored at the cell faces. The pressure-velocity coupling is obtained using the SIMPLEC algorithm [24]. For the convective terms in eqs (1) and (2) hybrid differencing was used. The transient equations were solved with 0.01 s time steps until steady state is reached. A fully implicit backward differencing scheme was used for the time integration.

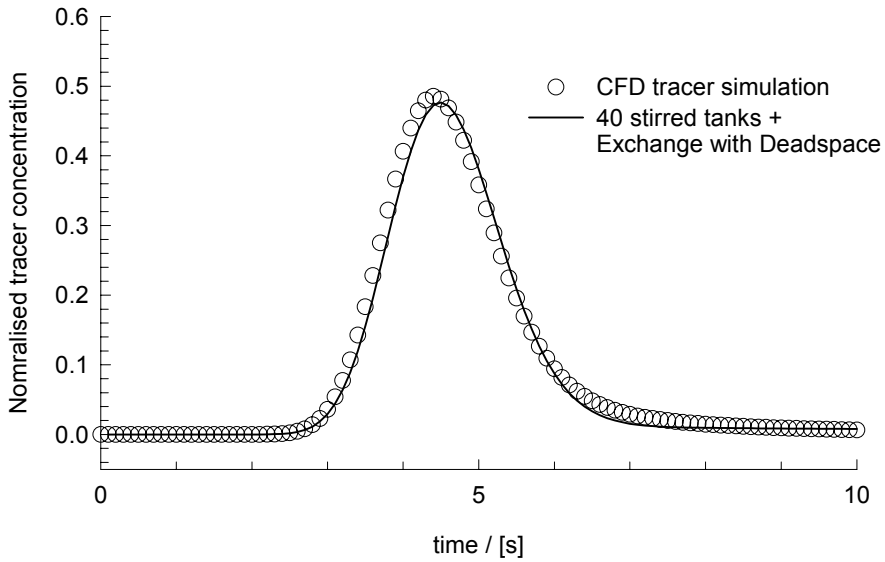

Figure 3. Residence time distribution obtained from pulse tracer injection CFD experiment shown in Fig. 2. The open circles represent the results of CFD simulations. The continuous lines represent the response calculated from a model in which N stirred tanks in series, including exchange with a dead zone.

The steady state velocity profiles are shown in Fig. 1 (b) and 1 (c). The recirculation patterns in the rounded segments of the tray are evident. Such recirculation patterns were first highlighted in the classic paper of Porter, Lockett and Lim [25]. We note from Fig. 1 (c) that the liquid velocity in the central flow path is about 0.06 m/s whereas the liquid is practically at a standstill in a major portion of rounded segments. CFD simulations can also be used to determine the residence time distribution by injecting a pulse tracer and monitoring its progression as it moves through the tray. Snapshots of the tracer movement are shown in Fig. 2. It is clearly seen that while the tracer concentration has reduced to practically zero in the central rectangular region within 8 s of tracer injection, it is swished to the rounded segmental regions and lingers there for a very long time. The normalized RTD is shown in Fig. 3. The tracer response cannot be described by an axial dispersion model; on the other hand a model with N stirred tanks in series, exchanging tracer with a dead space is able to match the tracer response very well; see the continuous lines in Fig. 3. The best fit with the CFD simulations is obtained taking the number of stirred tanks N = 40 and the dead space volume to be 28 % of the total tray volume.

The exchange between the active and the dead zone amounts to only 0.004 of the inlet flow. From geometry considerations the rounded segmental portions are 32% of the total tray volume; this is in close agreement with that determined from CFD simulations.

There are clear limitations of the above analysis assuming *two*-dimensional flow of only *liquid* across the tray. This is because the introduction of the gas phase will have a significant influence on the recirculation patterns. Furthermore, the gas-liquid hydrodynamics assumes a truly chaotic nature, as we shall see below.

3D SIMULATION STRATEGY FOR GAS-LIQUID HYDRODYNAMICS

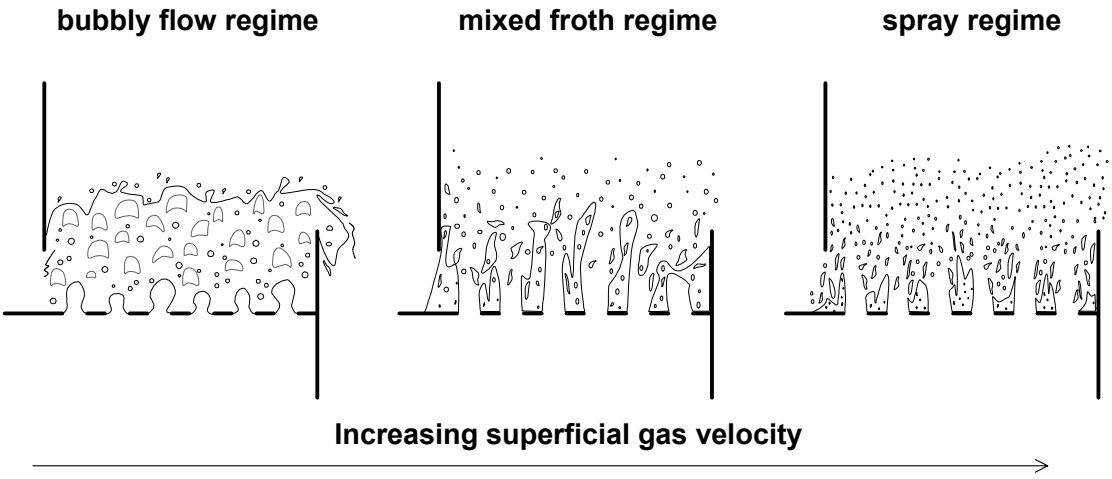

Figure 4. Flow regimes on sieve tray.

There are many flow regimes on sieve trays [2], ranging from gas-dispersed bubbly flow regime to liquid-dispersed spray flow regime; see Fig. 4. From a CFD point of view the bubbly flow regime is much easier to describe and model than the spray flow regime because it is easier to model the gas-liquid drag which is much more uniform along the dispersion height. On the other hand, in the spray flow regime, the gas-liquid drag can be expected to vary significantly up the dispersion, making the modelling much more difficult. We therefore restrict ourselves to the description of the bubbly flow regime. The derivation of the basic equations for dispersed two-phase flows is discussed by Jakobsen et al. [10] and here we present a summary. For either gas (subscript G) or liquid (subscript L) phases in the two-phase dispersion on the tray the volume-averaged mass and momentum conservation equations are given by:

$$\frac{\partial(\varepsilon_G \rho_G)}{\partial t} + \nabla \bullet (\rho_G \varepsilon_G \mathbf{u}_G) = 0 \tag{3}$$

$$\frac{\partial(\varepsilon_L \rho_L)}{\partial t} + \nabla \bullet (\rho_L \varepsilon_L \mathbf{u}_L) = 0 \tag{4}$$

$$\begin{aligned} &\frac{\partial(\rho_G \varepsilon_G \mathbf{u}_G)}{\partial t} + \nabla \bullet \left(\rho_G \varepsilon_G \mathbf{u}_G \mathbf{u}_G - \mu_G \varepsilon_G \left(\nabla \mathbf{u}_G + (\nabla \mathbf{u}_G)^{\mathrm{T}}\right)\right) \\ &\quad = -\varepsilon_G \nabla p + \mathbf{M}_{G,L} + \rho_G \varepsilon_G \mathbf{g} \end{aligned} \tag{5}$$

$$\frac{\partial(\rho_L \varepsilon_L \mathbf{u}_L)}{\partial t} + \nabla \bullet \left(\rho_L \varepsilon_L \mathbf{u}_L \mathbf{u}_L - \mu_L \varepsilon_L \left(\nabla \mathbf{u}_L + (\nabla \mathbf{u}_L)^{\mathrm{T}}\right)\right) = -\varepsilon_L \nabla p - \mathbf{M}_{G,L} + \rho_L \varepsilon_L \mathbf{g} \tag{6}$$

where ρ_k, $\mathbf{u}_k$, ε_k and μ_k represent, respectively, the macroscopic density, velocity, volume fraction and viscosity of the *k*th phase, *p* is the pressure, $\mathbf{M}_{G,L}$, the interphase momentum exchange between gas and liquid phases and **g** is the gravitational acceleration. The gas and liquid phases share the same pressure field, $p_G = p_L$. The added mass force has been ignored in the present analysis. Lift forces are also ignored in the present analysis because of the uncertainty in assigning values of the lift coefficients. For the continuous, liquid, phase, the turbulent contribution to the stress tensor is evaluated by means of *k*-ε model, using standard single-phase parameters. No turbulence model is used for calculating the velocity fields within the dispersed gas bubbles in the bubbly flow regime.

The interphase momentum exchange term is:

$$\mathbf{M}_{L.G} = \frac{3}{4} \rho_L \frac{\varepsilon_G}{d_G} C_D (\mathbf{u}_G - \mathbf{u}_L) |\mathbf{u}_G - \mathbf{u}_L| \tag{7}$$

where C_D is the interphase momentum exchange coefficient or drag coefficient. The proper estimation of the drag coefficient is the key to the successful modelling of the tray hydraulics. For the Stokes regime:

$$C_D = 24 / \mathrm{Re}_G; \quad \mathrm{Re}_G = \rho_L U_G d_G / \mu_L \tag{8}$$

and for the inertial regime, also known as the turbulent regime:

$$C_D = 0.44 \tag{9}$$

For the churn-turbulent regime of bubble column operation, Krishna et al. [12,14] estimated the drag coefficient for a swarm of large bubbles using:

$$C_D = \frac{4}{3} \frac{\rho_L - \rho_G}{\rho_L} g d_G \frac{1}{V_{slip}^2} \tag{10}$$

where V_{slip} is the slip velocity of the bubble swarm with respect to the liquid:

$$V_{slip} = |\mathbf{u}_G - \mathbf{u}_L| \tag{11}$$

Substituting eqs (10) and (11) into eq. (7) we find:

$$\mathbf{M}_{L.G} = \varepsilon_G (\rho_L - \rho_G) g \frac{1}{V_{slip}^2} (\mathbf{u}_G - \mathbf{u}_L) |\mathbf{u}_G - \mathbf{u}_L| \tag{12}$$

The slip between gas and liquid can be estimated from superficial gas velocity U_G and the gas hold-up ε_G:

$$V_{slip} = U_G / \varepsilon_G \tag{13}$$

An empirical correlation for the gas fraction on the tray as a function of the superficial gas velocity can be used to the estimate the slip velocity. In this work, we use the Bennett et al. [26] correlation to estimate the gas hold-up:

$$\varepsilon_L^B = \exp\left[-12.55\left(U_G\sqrt{\frac{\rho_G}{\rho_L-\rho_G}}\right)^{0.91}\right];\quad \varepsilon_G^B = 1-\varepsilon_L^B \tag{14}$$

It is important to note that the Bennett correlation does not include tray geometry or scale parameters. The interphase momentum exchange term is therefore:

$$\mathbf{M}_{L.G} = \varepsilon_G(\rho_L-\rho_G)g\frac{1}{\left(U_G/\varepsilon_G^B\right)^2}(\mathbf{u}_G-\mathbf{u}_L)|\mathbf{u}_G-\mathbf{u}_L| \tag{15}$$

This formulation however gives numerical difficulties because in the freeboard the liquid hold-up is zero. In order to overcome this problem we modify eq. (15) as follows:

$$\mathbf{M}_{L.G} = \varepsilon_G\varepsilon_L(\rho_L-\rho_G)g\left[\frac{1}{\left(U_G/\varepsilon_G^B\right)^2}\frac{1}{\varepsilon_L^B}\right](\mathbf{u}_G-\mathbf{u}_L)|\mathbf{u}_G-\mathbf{u}_L| \tag{16}$$

where the term $\left[\frac{1}{\left(U_G/\varepsilon_G^B\right)^2}\frac{1}{\varepsilon_L^B}\right]$ is estimated a priori from the Bennett relation (14). This approach ensures that the average gas hold-up in the gas-liquid dispersion on the froth conforms to experimental data over a wide range of conditions (as measured by Bennett et al. [26]). When incorporating eq. (16) for the gas-liquid momentum exchange within the momentum balance relations (5) and (6) the local, transient, values of $\mathbf{u}_G$, $\mathbf{u}_L$, ε_G and ε_L are used. A further point to note is that use of eq. (16) for the momentum exchange obviates the need for specifying the bubble size. Indeed, for the range of superficial gas velocities used in our simulations to be reported below, 0.5 – 0.7 m/s, we do not expect well-defined bubbles. The two-phase Eulerian simulation approach used here only requires that the gas phase is the dispersed phase; this dispersion could consist of either gas bubbles or gas jets, or a combination thereof.

Figure 5 shows the configuration of the system that has been simulated. The diameter of the tray is 0.3 m with a height of 0.12 m. The length of the weir is 0.18 m, giving a flow path length of 0.24 m. The chosen height of 0.12 m is sufficient to prevent liquid carryover out of the computational space. The liquid enters the tray through a rectangular opening that is 0.015 m high. The height of the weir is varied in the simulations and has the values of 60, 80 and 100 mm. The total number of grid cells used in the simulations is 48×60×24 = 69120; 48 cells in liquid flow direction, 60 cells in direction perpendicular to the liquid flow and 24 cells in the vertical direction. Figure 6 shows the layout of the distributor grid, which consists of 180 holes. The choice of the grid size is based on our experience gained in the modelling of fluidised beds and gas-liquid bubble columns operating in the churn-turbulent regime [12,14,16]. The use of warped square holes does not impact on the simulation results, because we use the Eulerian framework for describing either fluid phase.

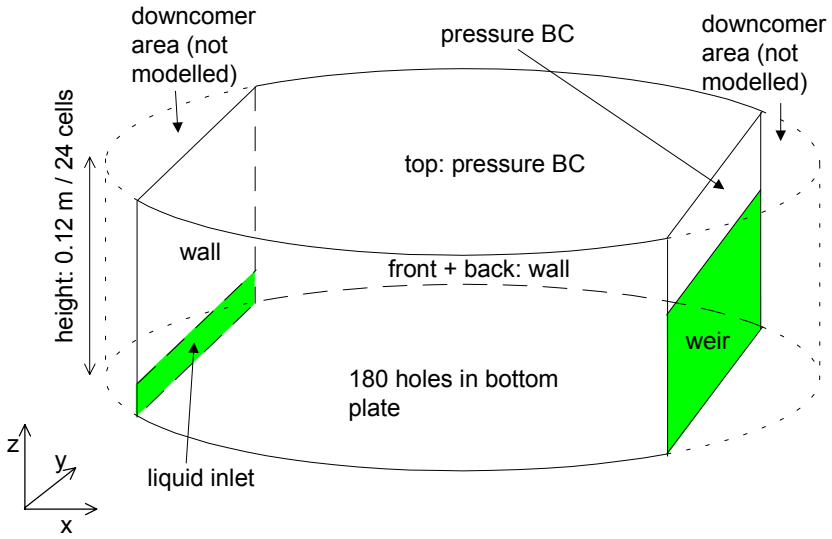

Figure 5. Specification of the computational space used in the CFD simulations. Total cross-sectional area of column = 0.07068 m^2; downcomer area = 0.003675 m^2; active bubbling area = 0.063 m^2; total number of holes = 180; hole area = 0.00414 m^2; fractional hole area to bubbling area = 6.54 %.

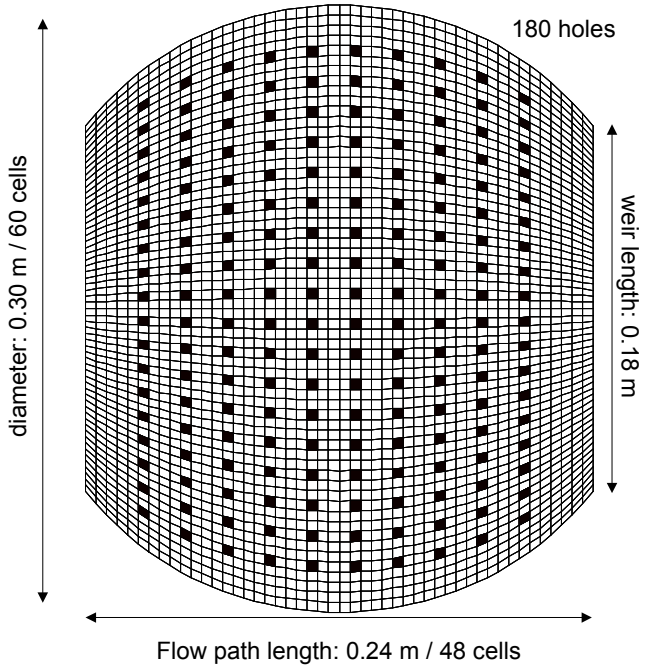

Figure 6. Layout of the distributor plate used in the CFD simulations: total number of holes = 180; hole area = 0.00414 m^2; fractional hole area to bubbling area = 6.54 %. The average area of one hole is 23 mm^2.

Air, at ambient pressure conditions, and water were used as the gas and liquid phases respectively. At the start of a simulation, the tray configuration shown in Fig. 5 is filled with a uniform gas-liquid dispersion, with 10% gas holdup, up to the height of the weir and gas is injected through the holes at the distributor. The time increment used in the simulations is 0.002 s. During the simulation the volume fraction of the liquid phase in the gas-liquid dispersion in the system is monitored and quasi-steady state is assumed to prevail if the value of the hold-up remains constant for a period long enough to determine the time-averaged values of the various parameters. For obtaining the values of the clear liquid height, gas holdup of dispersion, etc, the

parameter values are averaged over a sufficiently long period over which the holdup remains steady.

Simulations have been performed on a Silicon Graphics Power Challenge with six R10000 processors running at 200 MHz. A typical simulation took about 4 days to simulate 20 s of tray hydrodynamics. From the simulation results, average liquid hold-up as a function of height has been determined. Dispersion height has been defined by the height at which the average liquid hold-up drops below 10 percent. Clear liquid height has been determined by multiplying the average liquid hold-up with the height of the computational space (0.12 m). Further computational details of the algorithms used, boundary conditions, including animations are available on our web site: http://ct-cr4.chem.uva.nl/sievetrayCFD/.

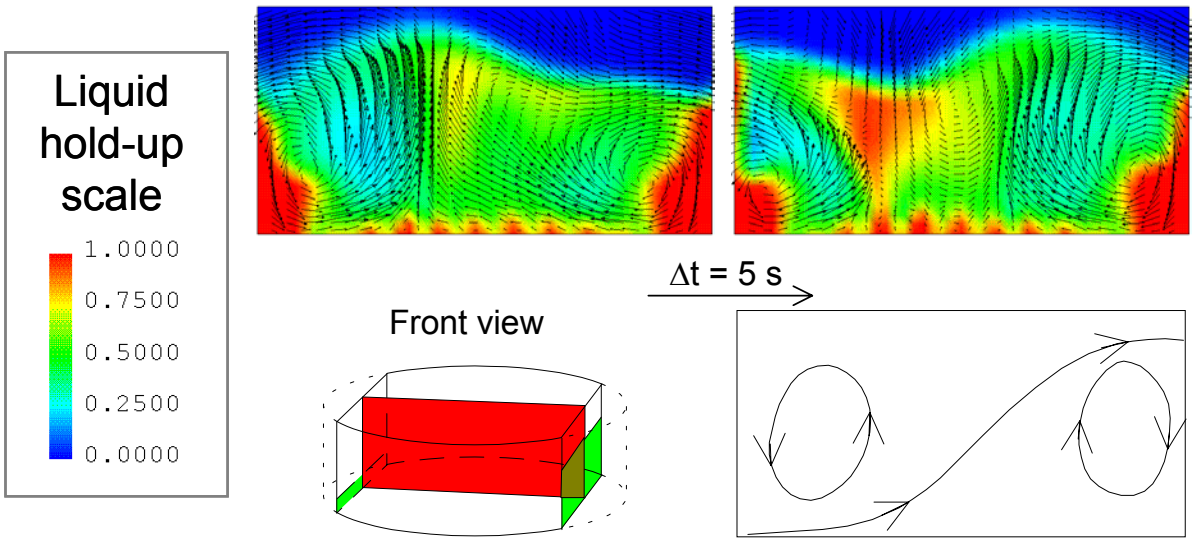

Figure 7. Snapshots of the front view of 0.3 m sieve tray simulations at a superficial gas velocity, U_G = 0.7 m/s; weir height h_w = 80 mm; liquid weir load $Q_L/W = 8.25\times10^{-4}$ $m^3/s/m$. The colours indicate the liquid holdup (scale on the left).

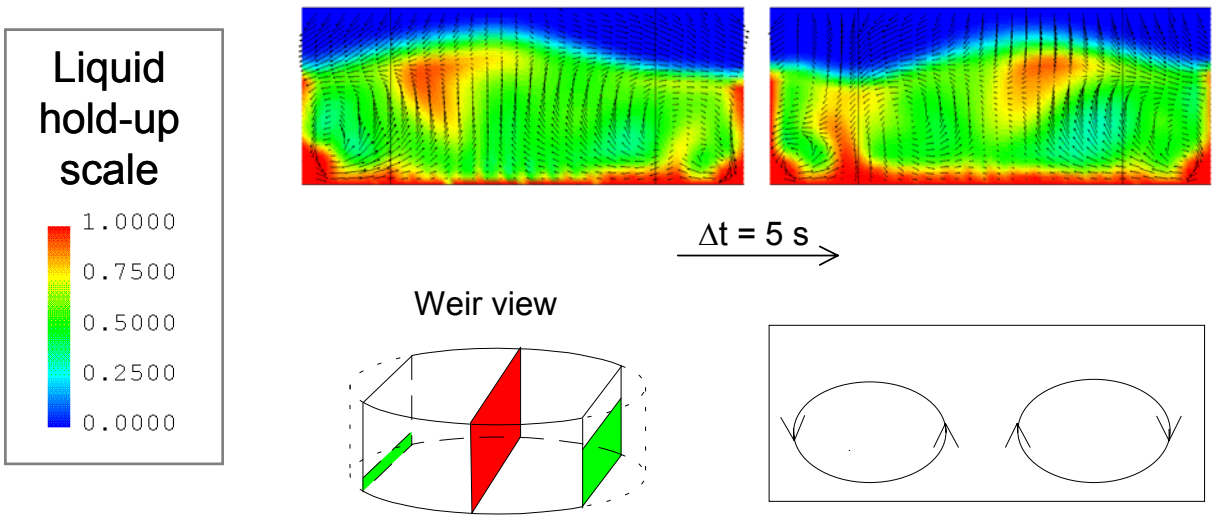

Figure 8. Snapshots of the weir view of 0.3 m sieve tray simulations at a superficial gas velocity, U_G = 0.7 m/s; weir height h_w = 80 mm; liquid weir load $Q_L/W = 8.25\times10^{-4}$ $m^3/s/m$. The colours indicate the liquid holdup (scale on the left).

Let us first consider snapshots, at 5 s intervals, of the movement of liquid along the flow path and over the weir; see Figs 7 and 8. Near the bottom of the tray, the liquid is drawn toward the centre and is dragged up vertically by the gas phase. The liquid disengages itself from the dispersed gas phase and travels down the sides, resulting in circulation cells that are evident in both the front (Fig. 7) and weir (Fig. 8) views. The snapshots also reflect the chaotic nature of the flow. There are two circulation cells when viewed from the front and from the weir.

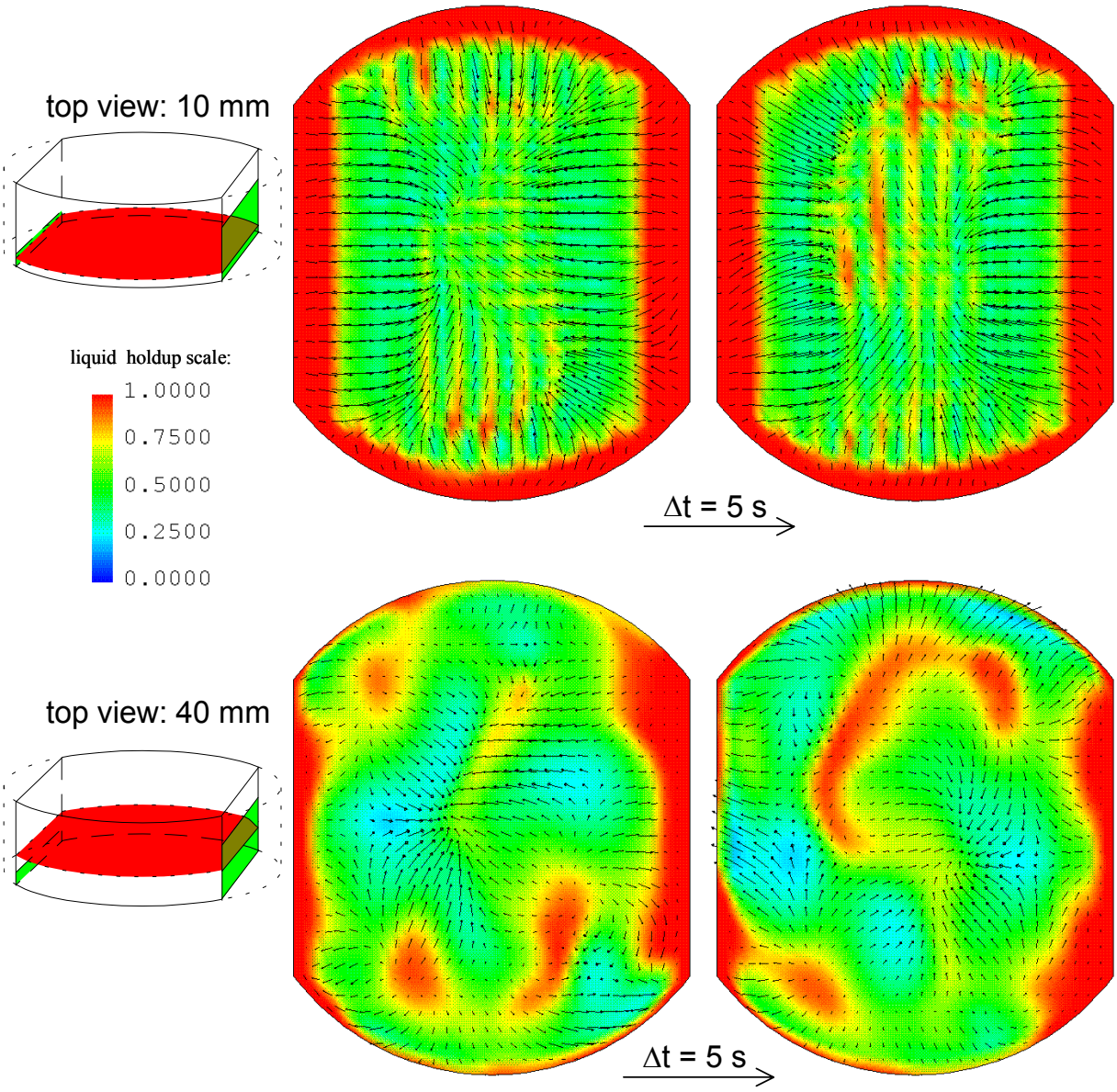

Figure 9. Snapshots of the top views, 10 and 40 mm above the floor of the 0.3 m tray. Superficial gas velocity, U_G = 0.7 m/s; weir height h_w = 80 mm; liquid weir load Q_L/W = 8.25×10^{-4} $m^3/s/m$. The colours indicate the liquid holdup (scale on the left).

Snapshots of the liquid flow patterns viewed 10 mm and 40 mm above the tray floor are shown in Fig. 9. Near the bottom of the tray the liquid is drawn inward and carried upwards; this is evidenced by the fact that all the liquid velocity vectors are pointing inwards; see 10 mm view at the top of the Fig. 9. Liquid recirculations are clearly

visible in the 40 mm view at the bottom of Fig. 9. The circulation patterns clearly have a chaotic character. When the transient simulations are time-averaged, the liquid phase velocity vectors at 40 mm above the tray are obtained as shown in Fig. 10. The recirculation cells at the rounded segments are clearly seen. However, it is interesting to note that the liquid velocity is directed towards the centre; this is because of the circulation cells seen in the front and weir views in Fig. 7 and 8 respectively. The liquid phase circulations *with gas flow* have therefore a totally different character than *without gas flow* (Fig. 2).

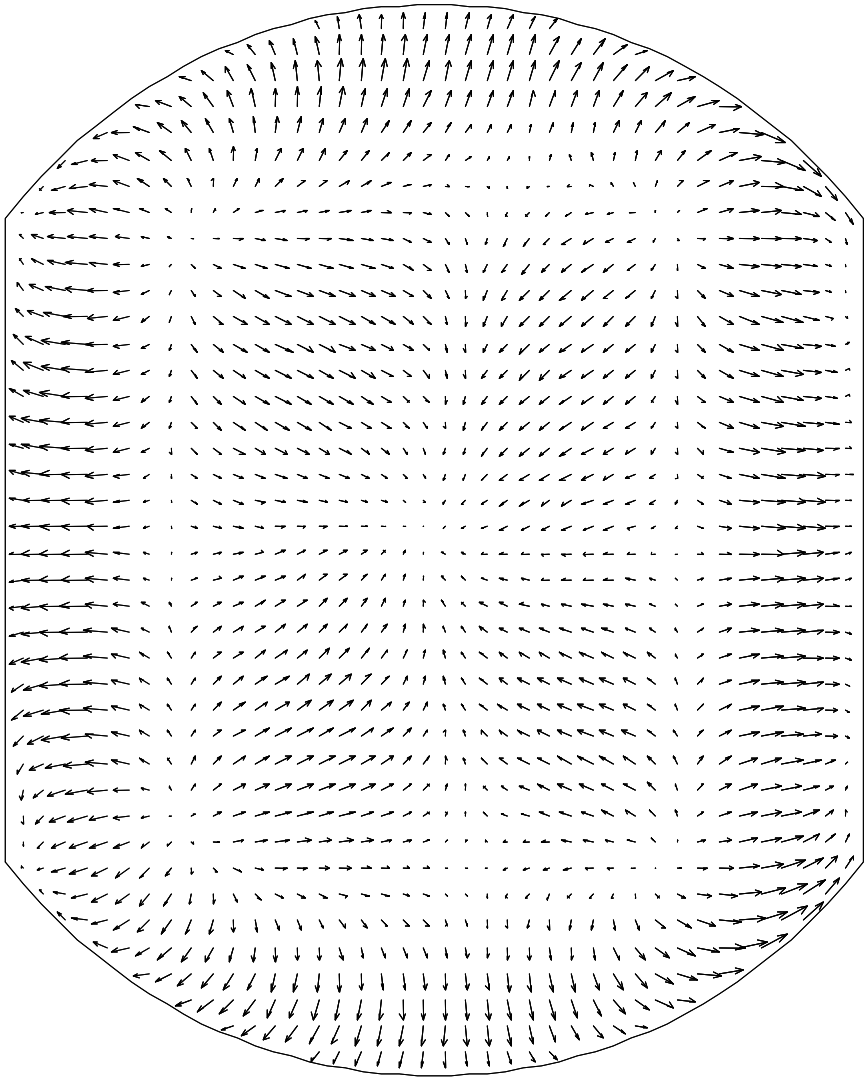

Figure 10. Time-averaged liquid phase velocity vectors, 40 mm above the floor of the 0.3 m tray. Superficial gas velocity, U_G = 0.7 m/s; weir height h_w = 80 mm; liquid weir load $Q_L/W = 8.25\times10^{-4}$ m^3/s/m.

Figure 11 presents typical simulation results for the variation of the liquid hold-up along the height of the dispersion. The values of the hold-up are obtained after averaging along the x- and y- directions and over a sufficiently long time interval once quasi-steady state conditions are established. The simulated trends in the liquid hold-up as a function of the gas velocity U_G are in line with literature information [27].

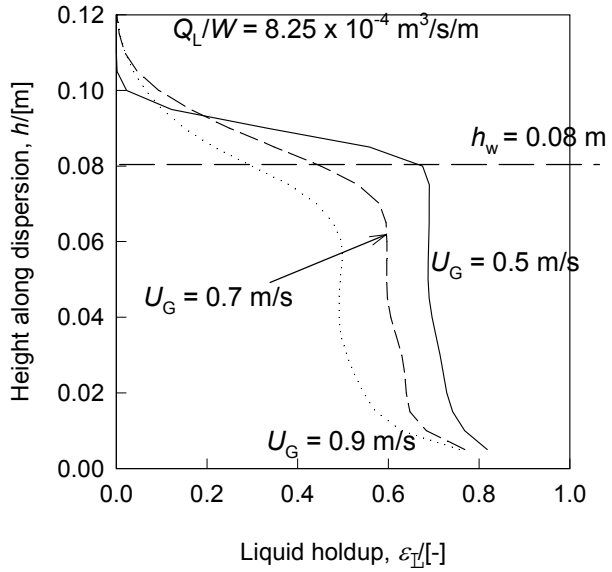

Figure 11. Distribution of liquid hold-up along the height of the dispersion for superficial gas velocities, U_G = 0.5, 0.7 and 0.9 m/s. Weir height h_w = 80 mm; liquid weir load $Q_L/W = 8.25 \times 10^{-4}$ m^3/s/m. The values of the hold-up are obtained after averaging along the x- and y- directions and over a sufficiently long time interval once quasi-steady state conditions are established.

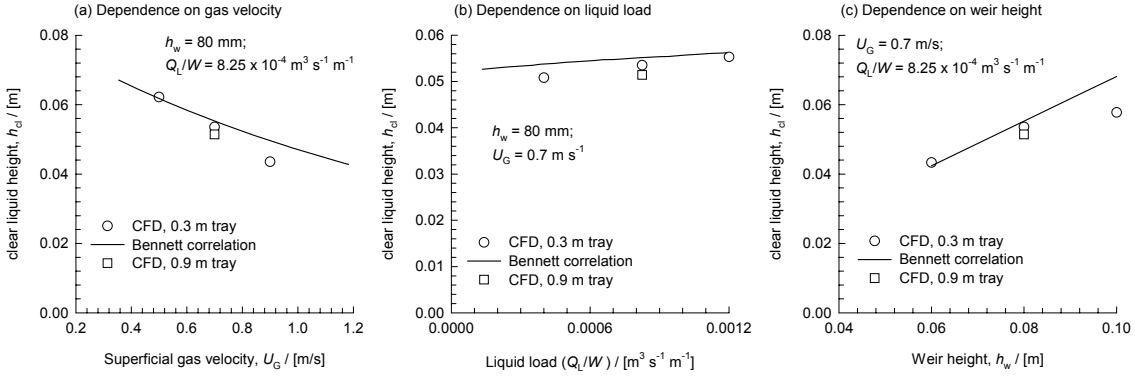

Figure 12. Clear liquid height as a function of the (a) superficial gas velocity, (b) liquid load, and (c) weir height. Comparison of Bennett correlation with CFD simulations for 0.3 m diameter tray. Also shown are CFD simulation results for 0.9 m tray (see below).

Figures 12 (a), (b) and (c) compare the calculations of the clear liquid height from CFD simulations with the Bennett correlation [26]:

$$h_{cl} = \varepsilon_L^B \left[h_w + C\left(\frac{Q_L}{W \varepsilon_L^B} \right)^{0.67} \right]; \quad C = 0.50 + 0.438 \exp(-137.8 h_w) \quad (17)$$

where ε_L^B is determined from eq. (14). It must be emphasised that eq. (17) is entirely independent of the holdup correlation presented in eq. (14). Put another way, the incoporation of the holdup correlation into our CFD inputs does not imply anything by way of information on the clear liquid height. The values of the clear liquid height

from the simulations are obtained after averaging over a sufficiently long time interval once quasi-steady state conditions are established and determining the cumulative liquid hold-up within the computational space. It is remarkable to note that the clear liquid height determined from the CFD simulations match the Bennett correlation quite closely, even though no influence of the weir height or liquid weir load on the interface gas-liquid momentum exchange coefficient has been used in the model. Geometry effects are properly taken account of in the CFD approach.

We have also studied the residence time distribution (RTD) of liquid phase by following the course of a tracer (red colour) in the liquid entering at the inlet to the tray. In order to gain insight into the tracer movement in the liquid phase let us consider a specific tray operation at U_G = 0.7 m/s, weir height h_w = 80 mm; liquid load Q_L/W = 8.25×10^{-4} m^3/s/m. Snapshots of the tracer concentrations are shown at 1 s, 5 s and 11 s from the start of the tracer injection are shown in Fig. 13. In sharp contrast to the corresponding 2D liquid simulations shown in Fig. 3, we note that the rounded segments have a high tracer concentration, 5 and 11 s after start of the simulation because of the liquid circulations. The conclusion to be drawn is that the existence of dead zones is not likely in actual practice.

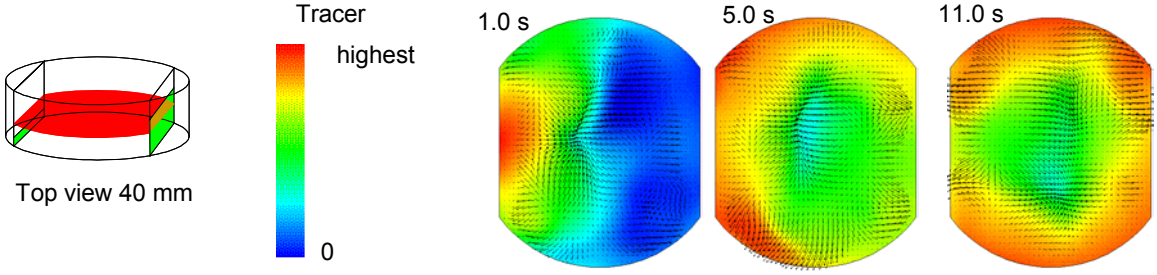

Figure 13. Snapshots of tracer concentration at 1, 5 and 11 s after tracer injection, viewed from the top at 40 mm above the floor of the 0.3 m tray. Superficial gas velocity, U_G = 0.7 m/s; weir height h_w = 80 mm; liquid weir load Q_L/W = 8.25×10^{-4} m^3/s/m. The colours indicate the liquid tracer concentration (see scale). Further computational details of the algorithms used, boundary conditions, including animations are available on our web site: http://ct-cr4.chem.uva.nl/sievetrayCFD/tracer/.

The major advantage of CFD simulations is that scale effects are captured. In order to illustrate this, let us consider simulations of at 0.9 m diameter tray operating at U_G = 0.7 m/s, weir height h_w = 80 mm; liquid load Q_L/W = 8.25×10^{-4} m^3/s/m. A total of 622080 cells are required to capture the hydrodynamics. A snapshot of the front view of the tray shows the existence of multiple cells, four in number, in the flow direction; see top of Fig. 14. This is in sharp contrast to the 0.3 m diameter tray, which displayed only two circulation cells in the flow direction. The weir view of the tray also shows the existence of four circulation cells; see bottom of Fig. 14.

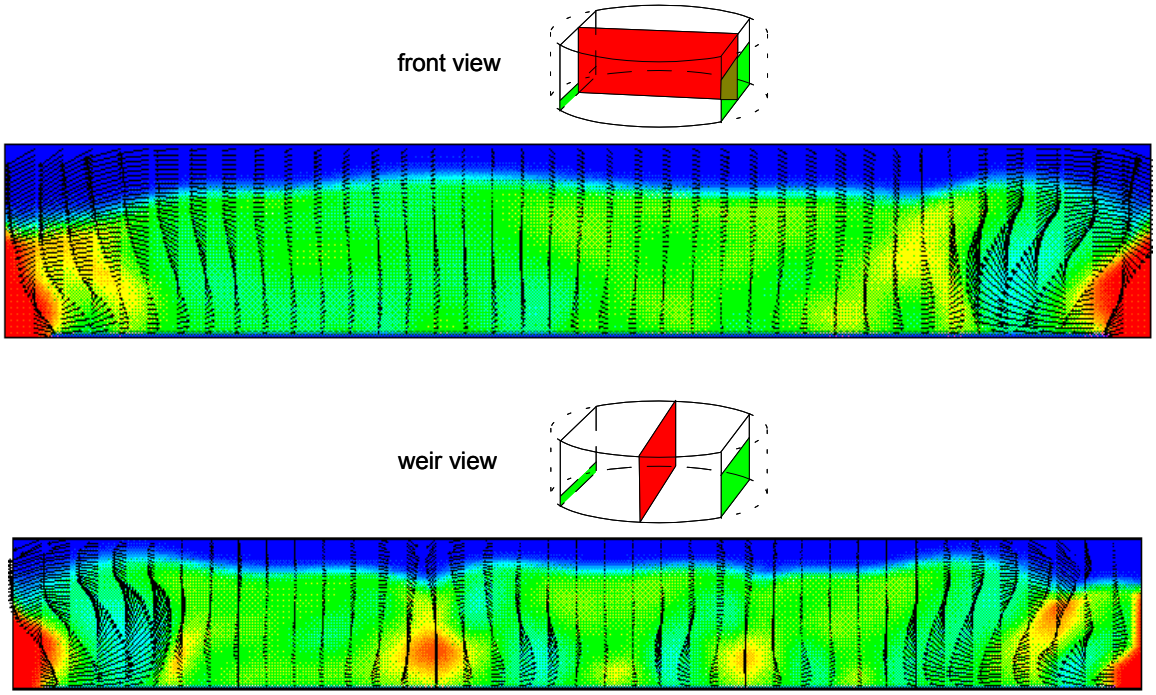

Figure 14a. Snapshots of the front view and weir view of 0.9 m sieve tray simulation at a superficial gas velocity, U_G = 0.7 m/s; weir height h_w = 80 mm; liquid weir load Q_L/W = 8.25×10^{-4} $m^3/s/m$. The colours indicate the liquid holdup (scale as in Fig. 7). Further computational details of the algorithms used, boundary conditions, including animations are available on our web site: http://ct-cr4.chem.uva.nl/sievetrayCFD/big/.

When the 0.9 m tray is viewed from the top at a position 40 mm above the tray floor, we again note a multiplicity of circulation patterns; see Fig. 15. It is clear that as the column diameter increases, so do the number of circulation cells. This implies that the liquid phase will be more backmixed in columns of smaller diameter. The liquid phase in large diameter columns can be taken to be in plug flow.

The time averaged clear liquid height, h_{cl}, for the 0.9 m tray after quasi-steady state has been achieved is almost identical to that of the 0.3 m diameter tray; the simulation results are compared in Fig. 12. There is apparently no scale effect with regard to clear liquid height and gas holdup on the tray. The mixing character of the liquid phase is however profoundly influenced by the scale, as has been emphasised above.

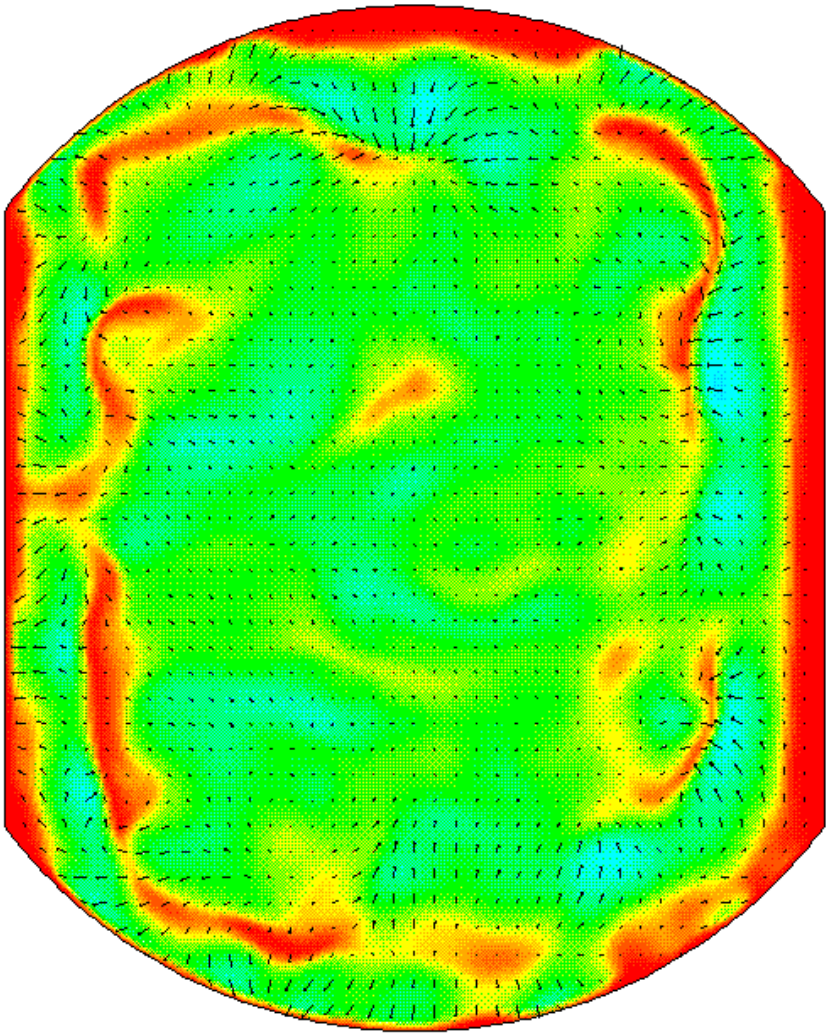

Figure 15. Snapshots of the top view, 40 mm above the tray floor, of 0.9 m sieve tray simulation at a superficial gas velocity, U_G = 0.7 m/s; weir height h_w = 80 mm; liquid weir load $Q_L/W = 8.25\times10^{-4}$ $m^3/s/m$. The colours indicate the liquid holdup (scale as in Fig. 7). See also our web site: http://ct-cr4.chem.uva.nl/sievetrayCFD/big/.

HYDRODYNAMICS OF SIEVE TRAYS WITH CATALYST CONTAINERS

There is a great deal of industrial interest in reactive distillation [28]. For heterogeneously catalysed liquid phase reactions, the liquid phase has to be brought into intimate contact with catalyst particles. Both packed columns (random packed or structured) and tray columns could be used. In order to avoid diffusional (diffusion limitations?) limitations the catalyst particles have to be smaller than about 3 mm in size. Such catalyst particles are usually encased within wire-gauze envelopes as in the KATAPAK-S and KATAMAX constructions of Sulzer Chemtech and Koch-Glitsch. An alternative to the KATAPAK-S and KATAMAX construction is to dispose the wire gauze parcels containing catalyst along the liquid flow direction of a sieve tray distillation column as shown in Fig. 16. The liquid hold-up is usually much higher in sieve tray columns as compared to packed columns and this is an advantage when carrying out relatively slow, catalysed, liquid phase reactions. A further advantage of a catalytic sieve tray construction is that the contacting on any tray is *cross-current* and for large diameter columns there will be a high degree of staging in the liquid

phase; this is advantageous from the point of view of selectivity and conversion. There is very little published information on the hydrodynamics of such contacting devices. CFD simulations are particularly suited to describe the hydrodynamics, because the preferred regime of operation in reactive distillation tray columns is the bubbly flow regime, which is well described in CFD as seen in the foregoing.

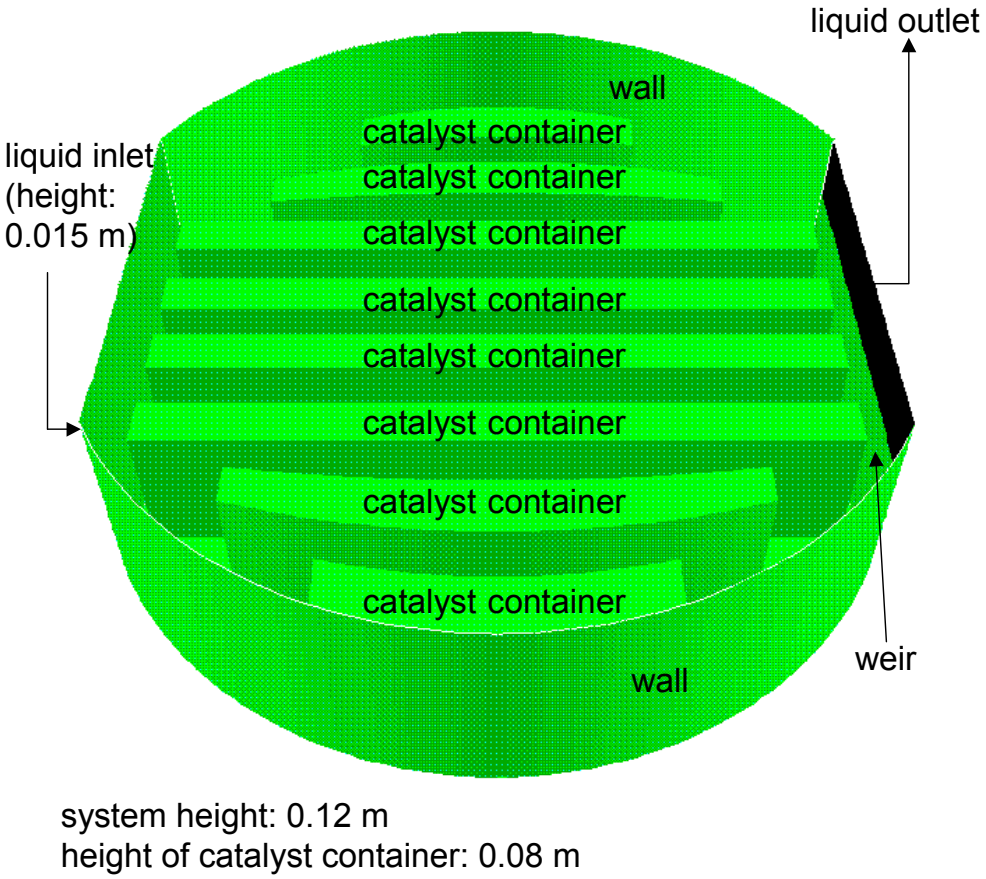

Figure 16. Computational space for CFD simulations 0.3 m diameter sieve tray containing catalyst filled containers.

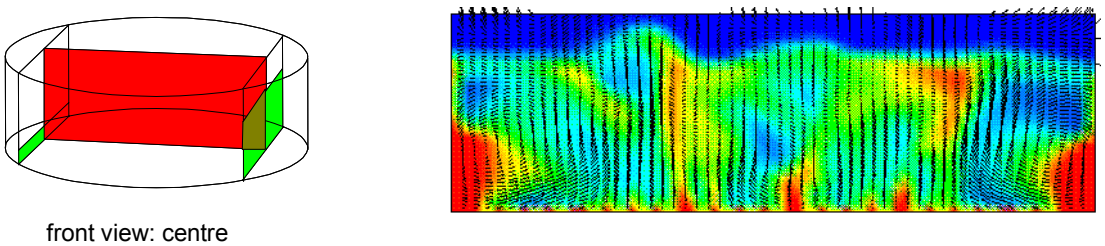

front view: centre

Figure 17. Snapshots of the front view of 0.3 m catalyst containing sieve tray simulations at a superficial gas velocity, U_G = 0.7 m/s; weir height h_w = 80 mm; liquid weir load $Q_L/W = 8.25 \times 10^{-4}$ $m^3/s/m$. The colours indicate the liquid holdup (scale as in Fig. 7). Animations can be viewed on our web site: http://ct-cr4.chem.uva.nl/katsievetrayCFD/.

The gas-liquid flow in the open spaces between the catalyst containers can be modelled in exactly the same manner as before [29]. When viewed from the front, the hydrodynamics has the same chaotic character as before (see Fig. 7), as is

evidenced in the snapshot shown in Fig. 17. There tends to be accumulation of liquid on top of the catalyst containers; this is evidenced by the snapshot taken from the front, at a position 25 mm off-centre; see Fig. 18.

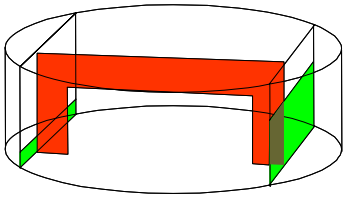

front view: 0.025 m (off-centre)

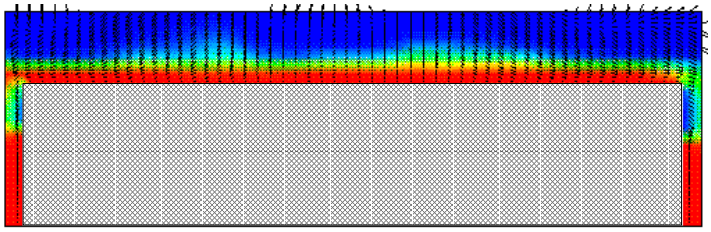

Figure 18. Snapshots of the front view of 0.3 m catalyst containing sieve tray simulations, off-centre front view. Operating conditions as in legend to Fig. 17. Animations can be viewed on our web site: http://ct-cr4.chem.uva.nl/katsievetrayCFD/.

The liquid accumulation is clearly evident in the snapshot taken from the weir view; see Fig. 20. The profiles of liquid holdup along the tray dispersion height shown in Fig. 21, shows clear differences with the corresponding simulations without containers shown in Fig. 11. In practice, this liquid accumulation can be prevented by tapering the top of the containers.

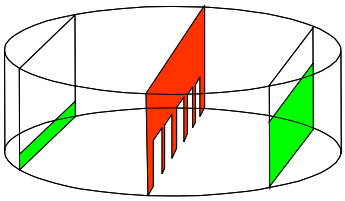

weir view: centre

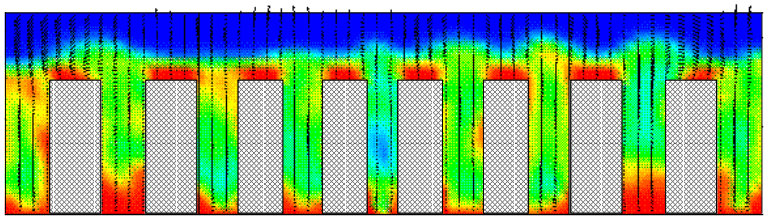

Figure 20. Snapshots of the weir view of 0.3 m catalyst containing sieve tray simulations. Operating conditions as in legend to Fig. 17. Animations can be viewed on our web site: http://ct-cr4.chem.uva.nl/katsievetrayCFD/.

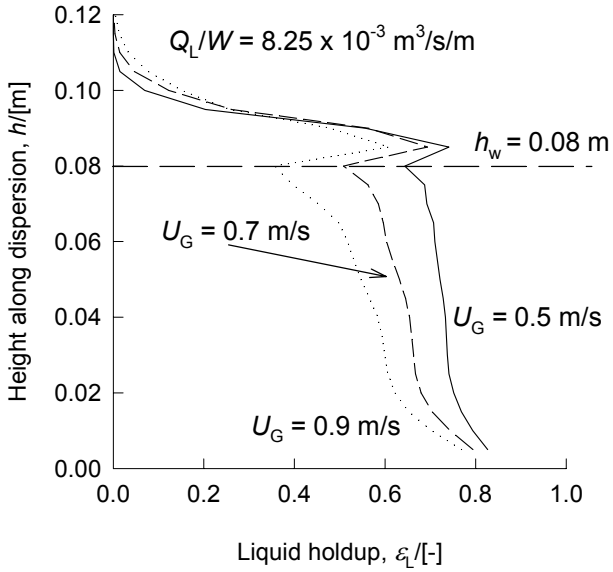

Figure 21. Simulation results with catalyst containers. Distribution of liquid hold-up along the height of the dispersion for superficial gas velocities, U_G = 0.5, 0.7 and 0.9 m/s. Weir height h_w = 80 mm; liquid weir load $Q_L/W = 8.25 \times 10^{-4}$ m^3/s/m. The corresponding simulation results without catalyst containers are shown in Fig. 11.

The presence of the liquid containers tends to dampen out the circulation cells and the flow along from the inlet to the weir has a more plug flow character; this is evidenced by the top view snapshot shown in Fig. 22.

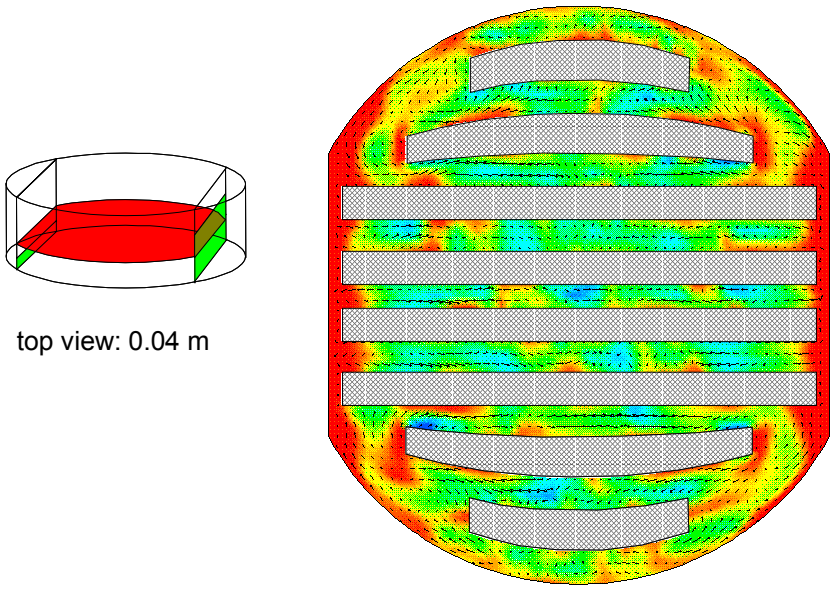

Figure 22. Snapshots of the top view of 0.3 m catalyst containing sieve tray simulations. Operating conditions as in legend to Fig. 17.

Good quantitative agreement between the CFD simulation results with catalyst containers and experimental results of Van Baten et al. [21,29], as is evidenced in the comparison presented in Fig. 23.

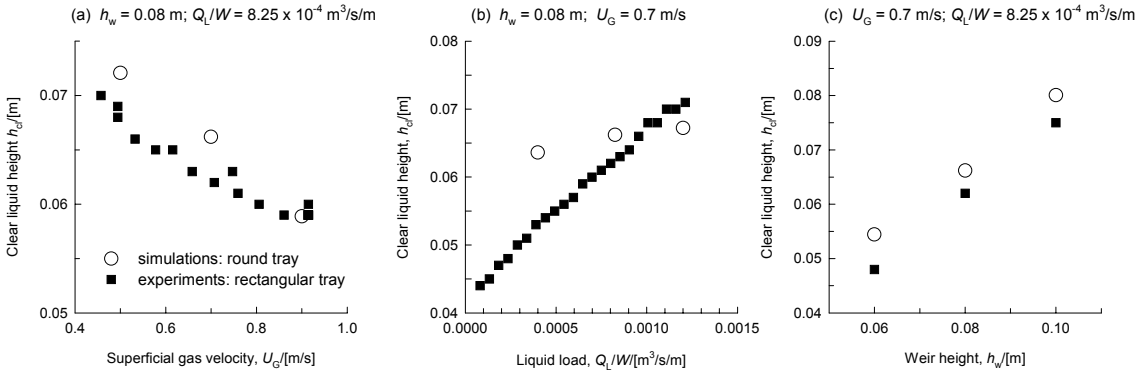

Figure 23. Experiments [21,29] vs. CFD simulations for hydrodynamics of sieve trays with catalyst containers. Clear liquid height as a function of the (a) superficial gas velocity, (b) liquid load, and (c) weir height.

CONCLUSIONS

We have discussed the modelling of the sieve tray hydrodynamics using CFD. Approaches, neglecting the gas phase and assuming the flow to be 2-dimensional in character exaggerate the importance of dead zones. A fully 3D transient simulation reveals the true three-dimensional and chaotic character with liquid circulation cells in both vertical and horizontal directions. The predictions of the clear liquid height and liquid hold-up from the CFD simulations show the right trends with varying superficial gas velocity, liquid weir load and weir height, and match the values of the Bennett correlation quite closely. The existence of dead zones is unlikely in actual practice. CFD simulations are able to describe the changes in the hydrodynamics with increasing scale. Comparing of the simulations of the 0.3 and 0.9 m diameter trays shows that the number of circulating cells increases with column diameter. This means that the liquid phase will tend to have a plug flow character in large diameter trays. The column diameter has however, a negligible effect on the clear liquid height and gas holdup on the tray.

CFD simulations are particularly helpful in describing the hydrodynamics of sieve trays containing internals such as catalyst containing envelopes.

Our studies show that CFD simulations can be a powerful investigative, and design tool for distillation trays. The success of the CFD technique is so far restricted to the bubbly flow regime. To describe the spray regime, more reliable models to represent the interphase drag coefficient will be required. This area requires further attention.

ACKNOWLEDGEMENT

The Netherlands Foundation for Scientific Research (NWO) is gratefully acknowledged for providing financial assistance in the form of a *programmasubsidie* for development of novel concepts in reactive separations technology.

NOTATION

d_G	diameter of gas bubble, m
C	parameter used in the Bennett correlation (17)
C_D	drag coefficient, dimensionless
g	acceleration due to gravity, 9.81 m/s^2
h_{cl}	clear liquid height, m
h_w	weir height, m
h	position along height, m
$\mathbf{M}$	interphase momentum exchange term, N/m^3
p	pressure, N/m^2
Q_L	liquid flow rate across tray, m^3/s
Re	Reynolds number, dimensionless
t	time, s
$\mathbf{u}$	velocity vector, m/s
U_G	superficial gas velocity, m/s
V_{slip}	slip velocity between gas and liquid, m/s
W	weir length, m
x	coordinate, m
y	coordinate, m
z	coordinate, m

Greek letters

ε	volume fraction of phase, dimensionless
μ	viscosity of phase, Pa s
ρ	density of phases, kg/m^3

Subscripts

cl	clear liquid
disp	dispersion
G	referring to gas phase
k	index referring to one of the phases
L	referring to liquid phase
slip	slip

Superscripts

B	from Bennett correlation

REFERENCES

1. *VISION 2020, 1998 Separations Roadmap*, Center for waste reduction technologies, A.I.Ch.E., New York, 1998.

2. Lockett, M.J., Distillation tray fundamentals, Cambridge university press, Cambridge (1986).

3. Kister, H.Z. Distillation design, McGraw-Hill, New York (1992).

4. Zuiderweg, F.J., Sieve trays. A view on the state of the art, *Chem. Eng. Sci.* **37** (1982) 1441 – 1464

5. Stichlmair, J.G. and Fair, J.R. *Distillation Principles and Practice*, Wiley-VCH, New York, 1998.

6. A.I.Ch.E. Bubble Tray Design Manual, A.I.Ch.E., New York (1958)

7. Fair, J.R., Steinmeyer, D.E., Penney, W.R. and Croker, B.B. Gas absorption and gas-liquid system design, Section 14 in Perry's Chemical Engineers' Handbook, D.W. Green and J.O. Maloney (editors), 7th Edition, McGraw-Hill, New York (1997)

8. Krishna, R. and Van Baten, J.M., Simulating the motion of gas bubbles in a liquid, *Nature***, 398** (1999) 208

9. Krishna, R., van Baten, J.M., Urseanu, M.I. and Ellenberger, J., Rise Velocity of Single Circular-Cap Bubbles in Two-dimensional Beds of Powders and Liquids, *Chem. Eng*. & *Processing*, **39** (2000) 433 - 440

10. Jakobsen, H.A., Sannæs, B.H., Grevskott, S., and Svendsen (1997), H.F. Modeling of bubble driven vertical flows. *Ind. Eng. Chem. Research*, 36**,** 4052-4074.

11. Borchersger, O., Busch, C., Sokolichin, A. and Eigenberger, G., Applicability of the standard k-ε turbulence model to the dynamic simulation of bubble columns: part II: comparison of detailed experiments and flow simulations, *Chem.Eng.Sci*, **54** (1999) 5927 - 5935*.*

12. Krishna, R. and van Baten, J.M., Scaling up bubble column reactors with the aid of CFD, *Chemical Engineering Research and Design, TransIChemE,* 79 (2001) 283-309

13. Thakre, S.S. and Joshi, J.B., CFD simulation of bubble column reactors: importance of drag force formulation, *Chem.Eng.Sci.*, **54** (1999) 5055-5060

14. Krishna, R., Van Baten, J.M. and Urseanu, M.I., Three-phase Eulerian simulations of bubble column reactors operating in the churn-turbulent flow regime: A scale up strategy, *Chem. Eng. Sci*., **55** (2000) 3275 - 3286

15. van Wachem, B.G.M., Schouten, J.C., van den Bleek, C.M., Krishna, R. and Sinclair, J.L. Comparative Analysis of CFD Models for dense Gas-Solid Systems, *A.I.Ch.E.J.*, **47** (2001) 1035-1051

16. Krishna, R., Van Baten, J.M., Using CFD for scaling up gas-solid bubbling fluidised bed reactors with Geldart A powders, *Chem.Eng. Journal*, **82** (2001) 247 - 257

17. Mehta, B., Chuang, K.T. and Nandakumar, K., Model for liquid phase flow on sieve trays, *Chem. Eng. Res. and Design, Trans. I.Chem.E.*, **76** (1998) 843- 848.

18. Liu, C.J., Yuan, X.G., Yu, K.T., Zhu, X.J., A fluid dynamic model for flow-pattern on distillation tray, *Chem. Eng. Sci.*, **55** (2000) 2287-2294

19. Krishna, R., Van Baten, J.M., Ellenberger, J., Higler, A.P. and Taylor, R., CFD simulations of sieve tray hydrodynamics, *Chem. Eng. Research & Design, Trans.I.Chem.E.*, **77** (1999) 639 - 646

20. Van Baten, J.M. and Krishna, R., Modelling of sieve tray hydraulics using computational fluid dynamics, *Chem. Eng. Journal*, **77** (2000) 143 - 152

21. van Baten, J.M., Ellenberger, J. and Krishna, R., Hydrodynamics of reactive distillation tray column with catalyst containing envelopes: Experiments vs. CFD simulations, *Catalysis Today*, **66** (2001) 233 - 240

22. B.E. Launder and B.T. Sharma "Application of the energy dissipationmodel of turbulence to the calculation of flow near a spinning disc", *Lett. Heat and Mass Transfer*, **1** (1974) 131-138.

23. Rhie, C.M. and Chow, W.L., Numerical study of the turbulent flow past an airfoil with trailing edge separation. *AIAA Journal.*, **21** (1983) 1525-1532.

24. Van Doormal, J. and Raithby, G.D. Enhancement of the SIMPLE method for predicting incompressible flows, *Numer. Heat Transfer*, **7**, 147-163 (1984),

25. Porter, K.E., Lockett, M.J. and Lim, C.T., The effect of liquid channelling on distillation plate efficiency, *Trans. I.Chem.E.*, **45**, (1972) 91 - 101.

26. Bennett D.L., Agrawal R., Cook P.J., New pressure drop correlation for sieve tray distillation columns. *A.I.Ch.E.J.,* 29 (1983) 434 - 442.

27. Hofhuis P.A.M, Zuiderweg F.J., Sieve plates: dispersion density and flow regimes. *Inst. Chem. Engrs. Symp. Series* No 56, 2.2/1 – 2.2/26 (1979).

28. R. Taylor and R. Krishna, Modelling reactive distillation, *Chem. Eng. Sci.,* **55** (2000) 5183 – 5229

29. J.M. van Baten, J. Ellenberger and R. Krishna, Hydrodynamics of distillation tray column with structured catalyst containing envelopes: Experiments vs. CFD simulations, *Chemical Engineering & Technology*, **24** (2001) 1077-1081